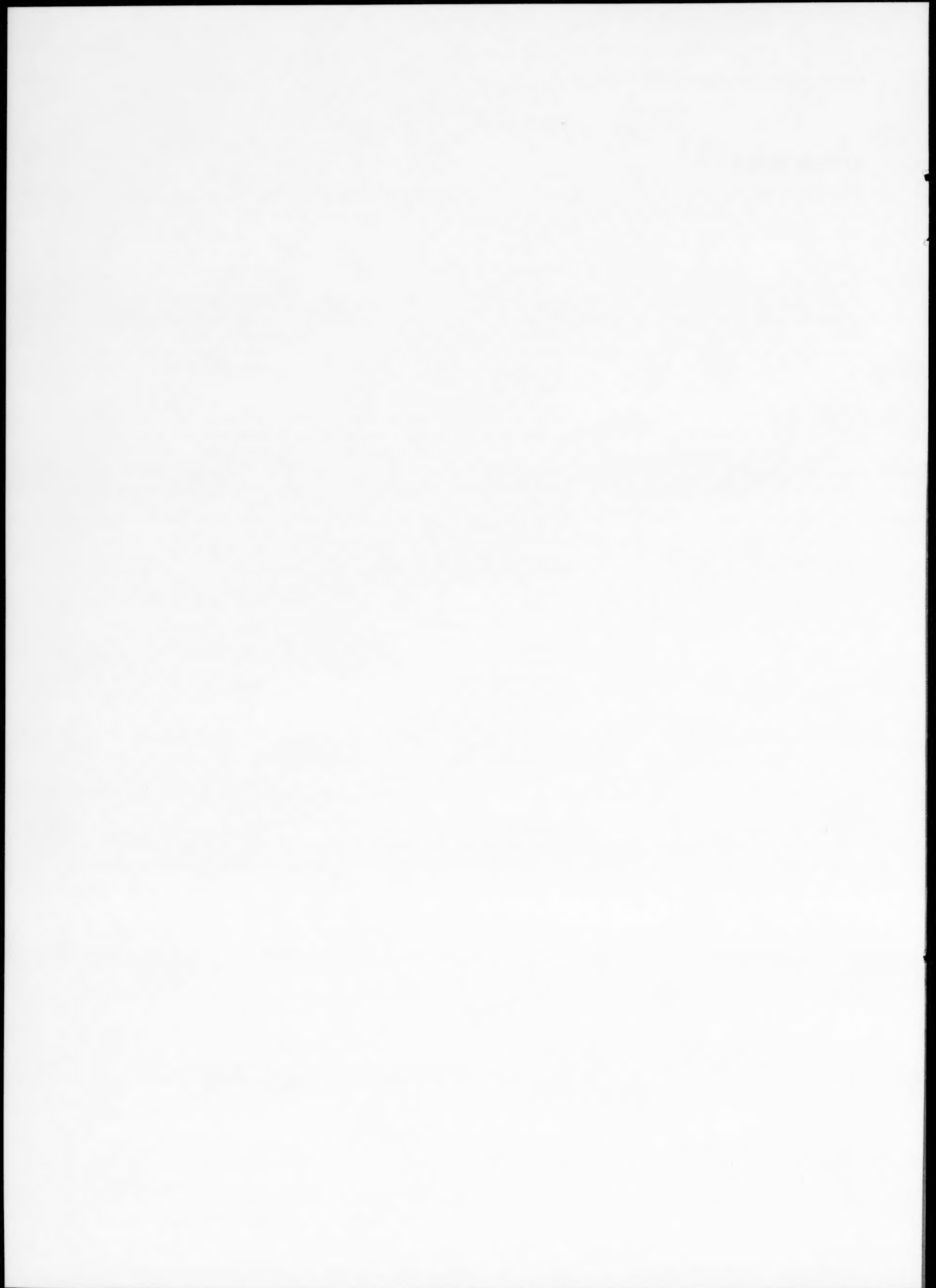


## Author Index

---

- Adams, B. L., 15  
Ahn, S., 255
- Bandyopadhyay, P. C., 245  
Bittner, J. C., 15  
Bowen, H. K., 235
- Case, E. D., 7  
Cejp, J., 153  
Cha, J. C., 121  
Chang, C.-M. R., L15  
Chaturvedi, M. C., 1  
Chiang, C. K., L27  
Chou, H. M., 7  
Chu, J., 31  
Cohen, J. B., 255
- Devgun, M. S., 129
- Fortes, M. A., 69  
Fowler, H. A., L27
- Gao, Y.-Q., 115  
Gawlik, G., 161  
Godowski, P., L19  
Gopalam, B. S. V., 241  
Grabski, M. W., 85, 93  
Gudmundsson, B., 207
- Herman, H., v  
Ho, N. J., 79  
Hua, M., L23  
Hwang, S. L., 177
- Iyer, K. J. L., L7
- Jacobson, B. E., 207  
Jagielski, J. J., 161  
Jain, A. K., 145  
Jena, A. K., 1  
Jiménez-Garay, R., 229  
Jin, Y., L23
- Karmazin, L., 201  
Kato, M., 31  
Khastgir, D., 245  
Kim, C. H., 121  
Kobayashi, T., 45  
Koczak, M. J., 37  
Kozubowski, J. A., 161  
Kuldeep, 145  
Kwon, H., 121
- Laird, C., 57  
Li, C., L23  
Lin, R.-S., L1  
Lunarski, J., 161
- Macek, K., 153  
Maiti, H. S., 245  
Markworth, A. J., 169  
Márquez, E., 229  
Melmed, A. J., L27  
Messerschmidt, U., 101  
Mulay, L. N., L11  
Murali, K. R., 241  
Murty, G. S., 37
- Nahass, P., 235  
Naidu, S. V., 187  
Niinomi, M., 45  
Nourbakhsh, S., 109
- O'Brien, T. D., 109
- Pak, H.-R., 31  
Pilling, J., 137  
Pluhar, J., 153  
Podgorski, A., 161  
Pope, D. P., 31
- Ritchie, R. O., 23  
Rolinski, E., 193  
Rosa, M. E., 69  
Rosenberg, Z., L9
- Sasaki, N., 45  
Sen, P., 187  
Senior, B. A., 219  
Serrano, J. R., L15  
Sharma, S. K., 145  
Shen, P., 177  
Shull, R. D., L27  
Swiatnicki, W. A., 85, 93
- Tjong, S. C., 79  
Tong, L.-Z., 115
- Varma, S. K., L15  
Venkateswara Rao, K. T., 23  
Villares, P., 229  
Viswanathan, S. K., 241
- Wang, W., 115  
Wang, Z., 57  
Wu, L. T., 79
- Yan, M., L23
- Zielinski, W., 161



## Subject Index

### Aging

aging and partial austenitizing of age-hardenable Cr-Ni-Mo steels of the type 10-10-2 and 6-11-3, 153

### Alloys

alloying behaviour of  $\text{Ni}_2\text{AlTi}$  and  $\text{NiAl}$  in yttria-partially stabilized zirconia, 177

effect of prolonged high-temperature exposure on the fatigue and fracture behavior of aluminum-lithium alloy 2090, 23

on electronic conduction in the pre-switching region of glassy semi-conducting alloys  $\text{As}_{40}\text{Se}_{30}\text{Te}_{30}$  and  $\text{As}_{20}\text{Se}_{50}\text{Te}_{30}$ , 229

some aspects of the dislocation microstructures in fatigued Fe-Cr-Al alloys, 79

some experiments and comments on the effect of hydrogen on the austenite to martensite transformation in a 1% carbon low alloy steel, L7

sulphur restraint of surface sites in Co-5.4at.%Ru alloy, L19

the multiple twinning of  $\text{Fe}_4\text{Al}_{13}$  as a heterogeneous phase in commercial Al-Zn-Mg-Cu alloys, L23

toughness and microstructural factors of Ti-6Al-4V alloy, 45

### Aluminium

alloying behaviour of  $\text{Ni}_2\text{AlTi}$  and  $\text{NiAl}$  in yttria-partially stabilized zirconia, 177

effect of prolonged high-temperature exposure on the fatigue and fracture behavior of aluminum-lithium alloy 2090, 23

some aspects of the dislocation microstructures in fatigued Fe-Cr-Al alloys, 79

structure formation and interdiffusion in vacuum plasma sprayed CoNiCrAlY coatings on IN738LC, 207

superplastic behavior of an Al-4wt.%Ti alloy processed by the powder metallurgy route, 37

the multiple twinning of  $\text{Fe}_4\text{Al}_{13}$  as a heterogeneous phase in commercial Al-Zn-Mg-Cu alloys, L23

toughness and microstructural factors of Ti-6Al-4V alloy, 45

### Amorphous

diffusion of antimony in amorphous and crystallized  $\text{Fe}_{82}\text{B}_{18}$ , 145

### Amorphous alloys

a model for the structures of amorphous metal-metalloid alloys, L1

### Annealing temperature

effect of annealing temperature on subgrain growth during recovery in OFHC copper, L15

### Antimony

diffusion of antimony in amorphous and crystallized  $\text{Fe}_{82}\text{B}_{18}$ , 145

### Arsenic

on electronic conduction in the pre-switching region of glassy semi-conducting alloys  $\text{As}_{40}\text{Se}_{30}\text{Te}_{30}$  and  $\text{As}_{20}\text{Se}_{50}\text{Te}_{30}$ , 229

### Austenite

some experiments and comments on the effect of hydrogen on the austenite to martensite transformation in a 1% carbon low alloy steel, L7

### Austenitic steel

effect of distribution of grain boundary diffusivity on plastic flow of austenitic steel

I: Characterization of microstructure. Determining the distribution of grain boundary diffusivity, 85

effect of distribution of grain boundary diffusivity on plastic flow of austenitic steel

II: The role of dislocation annihilation in grain boundaries in the plastic flow of polycrystalline materials, 93

### Austenitizing

aging and partial austenitizing of age-hardenable Cr-Ni-Mo steels of the type 10-10-2 and 6-11-3, 153

### Back stress

friction stress and back stress in cyclically deformed  $\text{Ni}_3\text{Ge}$  single crystals, 31

### Barium

the atomic fingerprint of  $\text{YBa}_2\text{Cu}_3\text{O}_{7-x}$ -type high-temperature superconductors observed by field ion microscopy, L27

### Boron

diffusion of antimony in amorphous and crystallized  $\text{Fe}_{82}\text{B}_{18}$ , 145

### Chrome

TEM studies of nitrides in surface-treated and implanted 12% chrome steel, 161

### Chromium

aging and partial austenitizing of age-hardenable Cr-Ni-Mo steels of the type 10-10-2 and 6-11-3, 153

some aspects of the dislocation microstructures in fatigued Fe-Cr-Al alloys, 79

### Cobalt

structure formation and interdiffusion in vacuum plasma sprayed CoNiCrAlY coatings on IN738LC, 207

sulphur restraint of surface sites in Co-5.4at.%Ru alloy, L19

### Copper

correlation of biaxial yield behavior in copper with crystallographic texture for strains in the range  $10^{-4}$ - $10^{-2}$ , 15

cyclic stress-strain response of polycrystalline copper under fatigue conditions producing enhanced strain localization, 57

effect of annealing temperature on subgrain growth during recovery in OFHC copper, L15

growth and characterization of  $\text{CuInSe}_2$  films by close-space evaporation, 241

the atomic fingerprint of  $\text{YBa}_2\text{Cu}_3\text{O}_{7-x}$ -type high-temperature superconductors observed by field ion microscopy, L27

- the multiple twinning of  $\text{Fe}_4\text{Al}_{13}$  as a heterogeneous phase in commercial Al-Zn-Mg-Cu alloys, L23
- Cork**  
temperature-induced alterations of the structure and mechanical properties of cork, 69
- Cryostat**  
a versatile cryostat and a mutual inductance coil for studying the Meissner effect in high  $T_c$  superconductors, L11
- Dielectric**  
polystyrene-titania composite as a dielectric material, 245
- Diffusion bonding**  
the kinetics of isostatic diffusion bonding in superplastic materials, 137
- Dislocation**  
effect of distribution of grain boundary diffusivity on plastic flow of austenitic steel  
II: The role of dislocation annihilation in grain boundaries in the plastic flow of polycrystalline materials, 93  
some aspects of the dislocation microstructures in fatigued Fe-Cr-Al alloys, 79  
line tension model of the interaction between dislocations and extended obstacles to glide, 101
- Elastic modulus**  
time-dependent recovery of the elastic modulus in thermally shocked polycrystalline yttrium iron garnet (YIG), 7
- Electronic conduction**  
on electronic conduction in the pre-switching region of glassy semi-conducting alloys  $\text{As}_{40}\text{Se}_{30}\text{Te}_{30}$  and  $\text{As}_{20}\text{Se}_{50}\text{Te}_{30}$ , 229
- Eutectoid gap**  
phase transformations of low-alloy steel at temperatures inside the eutectoid gap, 201
- Evaporation**  
growth and characterization of  $\text{CuInSe}_2$  films by close-space evaporation, 241
- Fatigue**  
cyclic stress-strain response of polycrystalline copper under fatigue conditions producing enhanced strain localization, 57  
effect of prolonged high-temperature exposure on the fatigue and fracture behavior of aluminum-lithium alloy 2090, 23  
some aspects of the dislocation microstructures in fatigued Fe-Cr-Al alloys, 79
- Field ion microscopy**  
the atomic fingerprint of  $\text{YBa}_2\text{Cu}_3\text{O}_{7-x}$ -type high-temperature superconductors observed by field ion microscopy, L27
- Fracture**  
assessment of fracture characteristics with X-ray diffraction techniques, 129  
effect of prolonged high-temperature exposure on the fatigue and fracture behavior of aluminum-lithium alloy 2090, 23  
the effect of grain size on fracture behaviour in tempered martensite embrittlement for AISI 4340 steel, 121
- Friction stress**  
friction stress and back stress in cyclically deformed  $\text{Ni}_3\text{Ge}$  single crystals, 31
- Garnet**  
time-dependent recovery of the elastic modulus in thermally shocked polycrystalline yttrium iron garnet (YIG), 7
- Germanium**  
friction stress and back stress in cyclically deformed  $\text{Ni}_3\text{Ge}$  single crystals, 31
- Grain boundary diffusivity**  
effect of distribution of grain boundary diffusivity on plastic flow of austenitic steel  
I: Characterization of microstructure. Determining the distribution of grain boundary diffusivity, 85  
effect of distribution of grain boundary diffusivity on plastic flow of austenitic steel  
II: The role of dislocation annihilation in grain boundaries in the plastic flow of polycrystalline materials, 93
- Grain size**  
the effect of grain size on fracture behaviour in tempered martensite embrittlement for AISI 4340 steel, 121
- Hydrogen**  
some experiments and comments on the effect of hydrogen on the austenite to martensite transformation in a 1% carbon low alloy steel, L7
- Indium**  
growth and characterization of  $\text{CuInSe}_2$  films by close-space evaporation, 241
- Inductance coil**  
a versatile cryostat and a mutual inductance coil for studying the Meissner effect in high  $T_c$  superconductors, L11
- Iridium**  
the strain sensitivity coefficients of resistance of rhodium, iridium and  $\text{Pd}_{20}\text{Ag}_{80}$ , 115
- Iron**  
diffusion of antimony in amorphous and crystallized  $\text{Fe}_{82}\text{B}_{18}$ , 145  
some aspects of the dislocation microstructures in fatigued Fe-Cr-Al alloys, 79  
the multiple twinning of  $\text{Fe}_4\text{Al}_{13}$  as a heterogeneous phase in commercial Al-Zn-Mg-Cu alloys, L23  
time-dependent recovery of the elastic modulus in thermally shocked polycrystalline yttrium iron garnet (YIG), 7
- Line tension**  
line tension model of the interaction between dislocations and extended obstacles to glide, 101
- Lithium**  
effect of prolonged high-temperature exposure on the fatigue and fracture behavior of aluminum-lithium alloy 2090, 23
- Magnesium**  
the multiple twinning of  $\text{Fe}_4\text{Al}_{13}$  as a heterogeneous phase in commercial Al-Zn-Mg-Cu alloys, L23
- Magnetite**  
the distribution of  $\Sigma$  boundaries in sintered magnetite, 255
- Martensite**  
on the effect of the volume fraction of martensite on the tensile strength of dual-phase steel, 1  
some experiments and comments on the effect of hydrogen on the austenite to martensite transformation in a 1% carbon low alloy steel, L7  
the effect of grain size on fracture behaviour in tempered martensite embrittlement for AISI 4340 steel, 121



**Meissner effect**

- a versatile cryostat and a mutual inductance coil for studying the Meissner effect in high  $T_c$  superconductors, L11

**Molybdenum**

- aging and partial austenitizing of age-hardenable Cr-Ni-Mo steels of the type 10-10-2 and 6-11-3, 153
- surface erosion study of alpha-bombarded molybdenum by scanning electron microscopy, 187

**Multiple surface-nucleation**

- a kinematical model of liquid-drop solidification due to multiple surface-nucleation events, 169

**Multiple twinning**

- the multiple twinning of  $\text{Fe}_4\text{Al}_{13}$  as a heterogeneous phase in commercial Al-Zn-Mg-Cu alloys, L23

**Nickel**

- aging and partial austenitizing of age-hardenable Cr-Ni-Mo steels of the type 10-10-2 and 6-11-3, 153
- alloying behaviour of  $\text{Ni}_2\text{AlTi}$  and  $\text{NiAl}$  in yttria-partially stabilized zirconia, 177
- friction stress and back stress in cyclically deformed  $\text{Ni}_3\text{Ge}$  single crystals, 31
- structure formation and interdiffusion in vacuum plasma sprayed CoNiCrAlY coatings on IN738LC, 207

**Nitrides**

- TEM studies of nitrides in surface-treated and implanted 12% chrome steel, 161

**Oxygen**

- the atomic fingerprint of  $\text{YBa}_2\text{Cu}_3\text{O}_{7-x}$ -type high-temperature superconductors observed by field ion microscopy, L27

**Palladium**

- strain sensitivity coefficients of resistance of rhodium, iridium and  $\text{Pd}_{20}\text{Ag}_{80}$ , 115

**Plasma**

- structure formation and interdiffusion in vacuum plasma sprayed CoNiCrAlY coatings on IN738LC, 207

**Plasma nitriding**

- mechanism of high-temperature plasma nitriding of titanium, 193

**Plastic flow**

- effect of distribution of grain boundary diffusivity on plastic flow of austenitic steel
  - I: Characterization of microstructure. Determining the distribution of grain boundary diffusivity, 85
- effect of distribution of grain boundary diffusivity on plastic flow of austenitic steel
  - II: The role of dislocation annihilation in grain boundaries in the plastic flow of polycrystalline materials, 93

**Polystyrene**

- polystyrene-titania composite as a dielectric material, 245

**Precipitation**

- precipitation of titania in a continuous-flow reactor with an organic base stabilizer, 235

**Resistance**

- on the elastic strain coefficients of resistance of metals, L9
- the strain sensitivity coefficients of resistance of rhodium, iridium and  $\text{Pd}_{20}\text{Ag}_{80}$ , 115

**Rhodium**

- the strain sensitivity coefficients of resistance of rhodium, iridium and  $\text{Pd}_{20}\text{Ag}_{80}$ , 115

**Ruthenium**

- sulphur restraint of surface sites in Co-5.4at.%Ru alloy, L19

**Scanning electron microscopy**

- surface erosion study of alpha-bombarded molybdenum by scanning electron microscopy, 187

**Selenium**

- growth and characterization of  $\text{CuInSe}_2$  films by close-space evaporation, 241
- on electronic conduction in the pre-switching region of glassy semi-conducting alloys  $\text{As}_{40}\text{Se}_{30}\text{Te}_{30}$  and  $\text{As}_{20}\text{Se}_{50}\text{Te}_{30}$ , 229

**Sigma boundaries**

- the distribution of  $\Sigma$  boundaries in sintered magnetite, 255

**Silver**

- the strain sensitivity coefficients of resistance of rhodium, iridium and  $\text{Pd}_{20}\text{Ag}_{80}$ , 115

**Solidification**

- a kinematical model of liquid-drop solidification due to multiple surface-nucleation events, 169

**Steel**

- effect of distribution of grain boundary diffusivity on plastic flow of austenitic steel
  - I: Characterization of microstructure. Determining the distribution of grain boundary diffusivity, 85
  - effect of distribution of grain boundary diffusivity on plastic flow of austenitic steel
    - II: The role of dislocation annihilation in grain boundaries in the plastic flow of polycrystalline materials, 93
  - on the effect of the volume fraction of martensite on the tensile strength of dual-phase steel, 1
- phase transformations of low-alloy steel at temperatures inside the eutectoid gap, 201
- some experiments and comments on the effect of hydrogen on the austenite to martensite transformation in a 1% carbon low alloy steel, L7
- TEM studies of nitrides in surface-treated and implanted 12% chrome steel, 161
- the effect of grain size on fracture behaviour in tempered martensite embrittlement for AISI 4340 steel, 121

**Strain**

- correlation of biaxial yield behavior in copper with crystallographic texture for strains in the range  $10^{-4}$ - $10^{-2}$ , 15
- cyclic stress-strain response of polycrystalline copper under fatigue conditions producing enhanced strain localization, 57
- on the elastic strain coefficients of resistance of metals, L9
- the strain sensitivity coefficients of resistance of rhodium, iridium and  $\text{Pd}_{20}\text{Ag}_{80}$ , 115

**Strain localization**

- cyclic stress-strain response of polycrystalline copper under fatigue conditions producing enhanced strain localization, 57

**Stress**

- cyclic stress-strain response of polycrystalline copper under fatigue conditions producing enhanced strain localization, 57

**Subgrain growth**

- effect of annealing temperature on subgrain growth during recovery in OFHC copper, L15

**Sulphur restraint**

- sulphur restraint of surface sites in Co-5.4at.%Ru alloy, L19

**Superconductors**

a versatile cryostat and a mutual inductance coil for studying the Meissner effect in high  $T_c$  superconductors, L11  
the atomic fingerprint of  $\text{YBa}_2\text{Cu}_3\text{O}_{7-x}$ -type high-temperature superconductors observed by field ion microscopy, L27

**Superplastic**

superplastic behavior of an Al-4wt.%Ti alloy processed by the powder metallurgy route, 37  
the kinetics of isostatic diffusion bonding in superplastic materials, 137

**Surface erosion**

surface erosion study of alpha-bombarded molybdenum by scanning electron microscopy, 187

**Surface sites**

sulphur restraint of surface sites in Co-5.4at.%Ru alloy, L19

**Tellurium**

on electronic conduction in the pre-switching region of glassy semi-conducting alloys  $\text{As}_{40}\text{Se}_{30}\text{Te}_{30}$  and  $\text{As}_{20}\text{Se}_{50}\text{Te}_{30}$ , 229

**Tensile strength**

on the effect of the volume fraction of martensite on the tensile strength of dual-phase steel, 1

**Titania**

polystyrene-titania composite as a dielectric material, 245  
precipitation of titania in a continuous-flow reactor with an organic base stabilizer, 235

**Titanium**

alloying behaviour of  $\text{Ni}_2\text{AlTi}$  and  $\text{NiAl}$  in yttria-partially stabilized zirconia, 177  
mechanism of high-temperature plasma nitriding of titanium, 193  
superplastic behavior of an Al-4wt.%Ti alloy processed by the powder metallurgy route, 37  
texture formation and transition in cold-rolled titanium, 109

toughness and microstructural factors of Ti-6Al-4V alloy, 45

**Toughness**

toughness and microstructural factors of Ti-6Al-4V alloy, 45

**Transmission electron microscopy**

TEM studies of nitrides in surface-treated and implanted 12% chrome steel, 161

**Vanadium**

toughness and microstructural factors of Ti-6Al-4V alloy, 45

**Welds**

the solidification and in-service transformation behaviour of type 316 and 347 welds fabricated with type 321 plate, 219

**X-ray diffraction**

assessment of fracture characteristics with X-ray diffraction techniques, 129

**Yield**

correlation of biaxial yield behavior in copper with crystallographic texture for strains in the range  $10^{-4}$ - $10^{-2}$ , 15

**Yttria**

alloying behaviour of  $\text{Ni}_2\text{AlTi}$  and  $\text{NiAl}$  in yttria-partially stabilized zirconia, 177

**Yttrium**

structure formation and interdiffusion in vacuum plasma sprayed CoNiCrAlY coatings on IN738LC, 207  
the atomic fingerprint of  $\text{YBa}_2\text{Cu}_3\text{O}_{7-x}$ -type high-temperature superconductors observed by field ion microscopy, L27  
time-dependent recovery of the elastic modulus in thermally shocked polycrystalline yttrium iron garnet (YIG), 7

**Zinc**

the multiple twinning of  $\text{Fe}_4\text{Al}_{13}$  as a heterogeneous phase in commercial Al-Zn-Mg-Cu alloys, L23

**Zirconia**

alloying behaviour of  $\text{Ni}_2\text{AlTi}$  and  $\text{NiAl}$  in yttria-partially stabilized zirconia, 177

